# Stochastic diffusion of ions due to a finite set of lower hybrid waves

Lucio M. Tozawa and Luiz F. Ziebell
*Instituto de Física, UFRGS, Porto Alegre, RS, Brazil*
(Received 6 February 2002; revised manuscript received 26 April 2002; published 21 November 2002)

In this paper we generalize the discussion on stochastic diffusion of energetic ions by lower hybrid waves by considering a case where a set of waves with similar frequencies is present in the system. In the particular case of a finite number of coherent waves, we show that the threshold for stochastic diffusion is reduced in comparison with the threshold in the one-wave case, and that the ensuing particle diffusion in velocity space occurs in periodic bursts along the time evolution. In the more general case of a set of waves with random phases, we have obtained even more efficient long-term diffusion in velocity space, for the same number of waves, although the initial diffusion rate can be smaller than in the case of coherent waves.

DOI: 10.1103/PhysRevE.66.056409 PACS number(s): 52.35.Fp, 52.35.Qz

## I. INTRODUCTION

The possibility of stochastic ion diffusion by lower hybrid (LH) waves has been proposed and explained over two decades ago, when it was shown that the movement of an ion in a uniform magnetic field becomes stochastic in the presence of a perpendicularly propagating coherent electrostatic wave, if the wave amplitude exceeds a threshold [1,2]. When the stochasticity criteria is satisfied, the ions diffuse in velocity space and it is possible to derive a diffusion equation to describe the time evolution of the ion distribution function. Such a diffusion mechanism may have important consequences, as indicated by relatively recent experiments, which have obtained evidence of interaction between lower hybrid waves and energetic ions in large tokamaks [3,4].

In a previous approach to the subject of interaction between energetic ions and LH waves in tokamak plasmas, we studied the parametric dependence of the threshold condition, and we have shown that the threshold condition as obtained in Ref. [1] may not be easily satisfied in present day large tokamaks, but can be attained in small tokamaks with relatively modest levels of wave power [5].

In another approach, we studied the same kind of interaction using a numerical analysis based on a quasilinear formalism appropriate for the situation in which ion stochastic diffusion occurs. The results obtained have shown significant wave-particle interaction taking place when a population of energetic ions is present in the plasma, in partial agreement with the evidence from experimental results available in the literature [6]. Proceeding with the investigation of the subject, in Ref. [7] we considered a case where a spectrum of low-intensity LH waves is present in the plasma, granting the use of quasilinear theory. The numerical implementation of the formalism has been considerably modified relatively to the previous formulation. In particular, in Ref. [7] the profile of energy deposition on the electron and ion distributions has been self-consistently evaluated for LH waves. In this investigation conducted in Ref. [7], as well as in Ref. [6], the energetic ion population was generated by a model term describing ion cyclotron (IC) waves, which was not self-consistent. The spatial distribution of IC wave power has been simply assumed as independent of the quasilinear evolution of the distribution function.

In this paper, we investigate the transition between these two situations, namely, the transition from the one-wave situation to the continuous wave spectra situation, and consider the appearance of stochasticity along this transition. This is accomplished through the generalization of Karney's approach to the case in which a finite number of waves is present in the system. The generalization can be made formally quite straightforward by the assumption of a simplifying hypothesis that the waves form a sufficiently narrow wave packet in **k** space. Despite the relative simplicity of the Hamiltonian obtained, the system dynamics is complicated and gives rise to interesting behavior, which has not up to the present been widely studied in the literature [8], although some relatively recent papers can be mentioned as dealing with different features of the subject [9,8,10].

The structure of the paper is the following. In Sec. II, we explain the fundamental features of the system and derive the equations of motion. In Sec. III, we present some numerical results that illustrate the appearance of stochastic diffusion in the system due to the presence of a set of lower hybrid waves, considering both the particular case of coherent waves and the more general case of waves with random phases. Finally, in Sec. IV, we summarize our findings and comment on the main results of the paper.

## II. THE DESCRIPTION OF THE SYSTEM AND THE EQUATIONS OF MOTION

Let us, therefore, consider the following magnetized system:

$$\mathbf{B}=B_0\mathbf{e}_z\,,$$

$$\mathbf{E}=\sum_i E_i(\omega_i)\cos[k_i(w_i)y-\omega_i t-\phi_i]\mathbf{e}_y\,. \tag{1}$$

The $\omega_i$ appearing in this expression are angular frequencies of the individual waves in a set of $n_\omega$ waves, the $E_i(\omega_i)$ are the amplitudes of these waves, and the $\phi_i$ are their phases.

Assuming the Coulomb gauge,

$$\mathbf{A}=-B_0 y\mathbf{e}_x\,,$$

we can write $\mathbf{E}=-\nabla\Phi$, with

 

$$\Phi = -\sum_i \frac{E_i(\omega_i)}{k_i(\omega_i)} \sin[k_i(w_i)y - \omega_i t - \phi_i]\mathbf{e}_y . \tag{2}$$

The Hamiltonian for the system can be written as

$$h = \frac{P^2}{2m} + q\Phi, \tag{3}$$

where

$$P^2 = p_x^2 + p_y^2 + q^2 B_0^2 y^2 - 2qp_x B_0 y,$$

and where $q$ and $m$ are the ion charge and mass, respectively, and the $p_i$ are the Cartesian components of the particle momentum. We have used $p_z(t=0)=0$, which implies $p_z(t)=0$.

For the sake of simplicity, we consider that $n_\omega$ is an odd number, with waves equally spaced in frequency. We denote the amplitude, the angular frequency, and the phases of the central wave as $\overline{E}$, $\overline{\omega}$, and $\overline{\phi}$, respectively, and assume initial conditions such that the phase of the central wave is zero ($\overline{\phi}=0$). Using these definitions, we introduce the dimensionless variables

$$t' = \Omega t, \quad \Omega = \frac{qB_0}{m}, \quad y' = \overline{k}y,$$

$$p_i' = \frac{\overline{k}}{m\Omega} p_i \quad (i = x,y), \tag{4}$$

where $\overline{k} = k_i(\omega_i = \overline{\omega})$.

As a consequence of these definitions, the Hamiltonian appears as

$$h' = \tfrac{1}{2}[(p_x' + y')^2 + p_y'^2] - \alpha \sum_i \frac{r_{E_i}}{r_{k_i}} \sin(r_{k_i} y' - \nu_i t' - \phi_i), \tag{5}$$

where

$$\alpha = \frac{qmE_0}{\overline{k}} \frac{\overline{k}^2}{m^2\Omega^2} = \frac{E_0}{B_0}\frac{\overline{k}}{\Omega} = \frac{E_0/B_0}{\Omega/\overline{k}},$$

$$r_{E_i} = \frac{E_i(\omega_i)}{E_0},$$

$r_{k_i} = k_i/\overline{k}$, $\nu_i = \omega_i/\Omega$, and $h' = hm/(m\Omega/\overline{k})^2$. The amplitude $E_0$ is obtained from the following normalization condition:

$$E_0^2 = 2\left\langle \left( \sum_i E_i \cos\varphi_i \mathbf{e}_y \right) \left( \sum_j E_j \cos\varphi_j \mathbf{e}_y \right) \right\rangle,$$

where $\varphi_i \equiv (k_i y - \omega_i t - \phi_i)$, and the symbol $\langle \cdots \rangle$ means the time average over a time interval sufficiently large in order to be an integer multiple of the periods of all waves appearing in the **k** wave packet. The rate of amplitudes $r_{E_i}$, therefore satisfies the following constraint:

$$\sum_{i=1}^{n_\omega} r_{E_i}^2 \langle \cos^2\varphi_i \rangle + 2 \sum_{i=1}^{n_\omega - 1} \sum_{j>i} r_{E_i} r_{E_j} \langle \cos\varphi_i \cos\varphi_j \rangle = \frac{1}{2}. \tag{6}$$

After performing the time average, we obtain $\langle \cos^2\varphi_i \rangle = 0.5$, and $\langle \cos\varphi_i \cos\varphi_j \rangle = 0.0$, and therefore, from Eq. (6),

$$\sum_{i=1}^{n_\omega} r_{E_i}^2 = 1. \tag{7}$$

In the case in which the $n_\omega$ waves of the **k** space packet have the same amplitude ($r_{E_i} = r_E$, for any $i$),

$$r_E = (n_\omega)^{-1/2}. \tag{8}$$

We can also define $r_{\omega_i} = \omega_i/\overline{\omega}$, and consider that the wave spectrum is nonvanishing only between $\overline{\omega} - \delta\omega$ and $\overline{\omega} + \delta\omega$, and therefore $r_{\omega_i}$ spreads from $r_{\omega_i} = 1 - \Delta$ to $r_{\omega_i} = 1 + \Delta$, where $\Delta = \delta\omega/\overline{\omega}$. Therefore, it is useful to introduce an integer index $i$ ranging from $-n_i$ to $n_i$, where $2n_i + 1 = n_\omega$, and write

$$r_{\omega_i} = 1 + i\Delta', \quad -n_i \leqslant i \leqslant n_i,$$

where $\Delta' = \Delta/n_i$.

If the wave packet in the **k** space is narrow, we may assume also for the sake of simplicity that for the waves in the packet

$$\frac{\omega}{k} \simeq V, \tag{9}$$

where $V$ is a constant. As a consequence,

$$r_{\omega_i} = \frac{\omega_i}{\overline{\omega}} = \frac{Vk_i(\omega_i)}{Vk_i(\overline{\omega})} = \frac{k_i(\omega_i)}{\overline{k}} = r_{k_i}(\omega_i),$$

and therefore

$$\nu_i = \frac{\omega_i}{\overline{\omega}} \frac{\overline{\omega}}{\Omega} = r_{k_i}\overline{\nu} \quad \text{where} \quad \overline{\nu} = \frac{\overline{\omega}}{\Omega}.$$

Dropping the ''primes,'' for simplicity, we obtain as the system's Hamiltonian,

$$h = \tfrac{1}{2}[(p_x + y)^2 + p_y^2] - \alpha \sum_i \frac{r_{E_i}}{r_{k_i}} \sin[r_{k_i}(y - \overline{\nu}t) - \phi_i]. \tag{10}$$

Following steps similar to those employed in Ref. [1], we perform the following canonical transformation:

$$(x, y, p_x, p_y) \Rightarrow (X, Y, P_x, P_y), \tag{11}$$

$$F_2(x, y, P_x, P_y) = (P_x - \overline{\nu}t)x + P_y(y - \overline{\nu}t + P_x),$$

$$X=\frac{\partial F_2}{\partial P_x}=x+P_y,$$

$$Y=\frac{\partial F_2}{\partial P_y}=y-\bar{\nu}t+P_x,$$

$$p_x=\frac{\partial F_2}{\partial x}=P_x-\bar{\nu}t,$$

$$p_y=\frac{\partial F_2}{\partial y}=P_y,$$

$$K=h+\frac{\partial F_2}{\partial t}=h-\bar{\nu}(x+P_y)=h-\bar{\nu}X,$$

resulting in

$$Y=y+p_x, \quad X=x+p_y.$$

The new Hamiltonian is

$$K(X,Y,P_x,P_y)=\tfrac{1}{2}[Y^2+P_y^2] - \alpha\sum_i \frac{r_{E_i}}{r_{k_i}}\sin[r_{k_i}(Y-P_x)-\phi_i]-\bar{\nu}X. \tag{12}$$

Performing now a second canonical transformation,

$$(X,Y,P_x,P_y)\Rightarrow(I_1,\omega_1,I_2,\omega_2),$$

$$F_1(X,Y,\omega_1,\omega_2)=\tfrac{1}{2}Y^2\cot(\omega_1)+X\omega_2,$$

$$P_x=\frac{\partial F_1}{\partial X}=\omega_2,$$

$$P_y=\frac{\partial F_1}{\partial Y}=Y\cot(\omega_1)\rightarrow P_y=(2I_1)^{1/2}\cos(\omega_1),$$

$$I_1=-\frac{\partial F_1}{\partial \omega_1}=\frac{1}{2}Y^2\,\mathrm{cosec}^2(\omega_1)\rightarrow Y=(2I_1)^{1/2}\sin(\omega_1),$$

$$I_2=-\frac{\partial F_1}{\partial \omega_2}=-X,$$

we arrive at the final form of the Hamiltonian, denoted as $H$,

$$H=K+\frac{\partial F_1}{\partial t}=K.$$

The Hamiltonian is therefore

$$H=I_1+\bar{\nu}I_2 - \alpha\sum_i \frac{r_{E_i}}{r_{\omega_i}}\sin\{r_{\omega_i}[R\sin(\omega_1)-\omega_2]-\phi_i\}, \tag{13}$$

where we have used $r_{k_i}=r_{\omega_i}$ and defined $R=(2I_1)^{1/2}$.

The Hamiltonian equations are easily obtained as follows:

$$\dot{\omega}_i=\frac{\partial H}{\partial I_i}, \quad \dot{I}_i=-\frac{\partial H}{\partial \omega_i},$$

$$\dot{\omega}_1=1-\sin(\omega_1)\frac{1}{R}\alpha\sum_i r_{E_i}\cos\{r_{\omega_i}[R\sin(\omega_1)-\omega_2]-\phi_i\},$$

$$\dot{\omega}_2=\bar{\nu},$$

$$\dot{I}_1=\cos(\omega_1)R\alpha\sum_i r_{E_i}\cos\{r_{\omega_i}[R\sin(\omega_1)-\omega_2]-\phi_i\},$$

$$\dot{I}_2=-\alpha\sum_i r_{E_i}\cos\{r_{\omega_i}[R\sin(\omega_1)-\omega_2]-\phi_i\}. \tag{14}$$

The Hamiltonian can be cast in a different form, which is more convenient for the ensuing analysis. We start again from Eq. (13), use $r_{\omega_i}=1+i\Delta'$, and define $\theta=R\sin(\omega_1)-\omega_2$, for simplicity,

$$H=I_1+\bar{\nu}I_2-\alpha\sum_i \frac{r_{E_i}}{(1+i\Delta')}\sin[(1+i\Delta')\theta-\phi_i]$$

$$=I_1+\bar{\nu}I_2-\alpha\sum_i \frac{r_{E_i}}{(1+i\Delta')}[\sin(\theta-\phi_i)\cos(i\Delta'\theta) + \cos(\theta-\phi_i)\sin(i\Delta'\theta)].$$

Since $\Delta'$ is a small quantity, we can, in principle, benefit from the following expansions:

$$\frac{1}{(1+i\Delta')}=\sum_{j=0}^{\infty}(-i\Delta')^j,$$

$$\cos(i\Delta'\theta)=\sum_{k=0}^{\infty}(-1)^k\frac{(i\Delta')^{2k}}{(2k)!}\theta^{2k},$$

$$\sin(i\Delta'\theta)=\sum_{k=0}^{\infty}(-1)^k\frac{(i\Delta')^{2k+1}}{(2k+1)!}\theta^{2k+1}.$$

The expansions for the trigonometric functions can be truncated only if the argument is sufficiently small. However, since $\omega_2=\bar{\nu}t+\mathrm{const}$, the argument is small only for times of order $t\leqslant 1/(\bar{\nu}\Delta)$. If, for instance, $\Delta=0.01$ and $\bar{\nu}=30$, that means $t\leqslant 3$. This is a very restrictive condition, which is not useful in the context of the present investigation. Therefore, we do not expand the trigonometric functions and write the Hamiltonian as follows:

$$H=I_1+\bar{\nu}I_2-\alpha\sum_{j=0}^{\infty}\sum_i r_{E_i}(-i\Delta')^j[\cos(i\Delta'\theta)\sin(\theta-\phi_i) + \sin(i\Delta'\theta)\cos(\theta-\phi_i)]. \tag{15}$$

Regarding the equations of motion, these can be derived from the Hamiltonian given by Eq. (15),

$$\dot{\omega}_1 = 1 - \alpha \frac{\partial \theta}{\partial I_1} \sum_{j=0}^{\infty} \sum_i r_{E_i} (-i\Delta')^j \{[\cos(i\Delta'\theta)\cos(\theta-\phi_i) - \sin(i\Delta'\theta)\sin(\theta-\phi_i)]$$

$$+ (i\Delta')[-\sin(i\Delta'\theta)\sin(\theta-\phi_i) + \cos(i\Delta'\theta)\cos(\theta-\phi_i)]\}$$

$$= 1 - \alpha \frac{\partial \theta}{\partial I_1} \sum_i r_{E_i} [\cos(i\Delta'\theta)\cos(\theta-\phi_i) - \sin(i\Delta'\theta)\sin(\theta-\phi_i)] \sum_{j=0}^{\infty} [(-i\Delta')^j - (-i\Delta')^{j+1}]$$

$$= 1 - \alpha \frac{\partial \theta}{\partial I_1} \sum_i r_{E_i} [\cos(i\Delta'\theta)\cos(\theta-\phi_i) - \sin(i\Delta'\theta)\sin(\theta-\phi_i)] \left[ 1 + \sum_{j=1}^{\infty} (-i\Delta')^j - \sum_{j=1}^{\infty} (-i\Delta')^j \right],$$

where we have used $j' = j+1$ in the last term, and then used $j' \to j$, for simplicity. Therefore,

$$\dot{\omega}_1 = 1 - \alpha \frac{1}{R} \sin(\omega_1) \sum_i r_{E_i} [\cos(i\Delta'\theta)\cos(\theta-\phi_i)$$

$$- \sin(i\Delta'\theta)\sin(\theta-\phi_i)]. \tag{16}$$

The other Hamiltonian equations can be easily obtained,

$$\dot{\omega}_2 = \overline{\nu},$$

$$\dot{I}_1 = \alpha R \cos(\omega_1) \sum_i r_{E_i} [\cos(i\Delta'\theta)\cos(\theta-\phi_i)$$

$$- \sin(i\Delta'\theta)\sin(\theta-\phi_i)],$$

$$\dot{I}_2 = -\alpha \sum_i r_{E_i} [\cos(i\Delta'\theta)\cos(\theta-\phi_i)$$

$$- \sin(i\Delta'\theta)\sin(\theta-\phi_i)]. \tag{17}$$

Equations (16) and (17) are completely equivalent to those appearing in Eqs. (14).

An interesting limiting case is obtained from the Hamiltonian (15) if $\Delta\theta$ is a small quantity, as it may occur for initial times in the case of narrow wave spectrum. In that case, the trigonometric functions can be expanded, and by neglecting terms of order $\Delta\theta$ and higher, the following approximated Hamiltonian is obtained:

$$H = I_1 + \overline{\nu} I_2 - \alpha \sum_i r_{E_i} \sin(\theta - \phi_i). \tag{18}$$

Particularly, if all waves in the wave spectrum have the same phase (for simplicity the same phase as the central wave, $\overline{\phi} = 0$), the Hamiltonian is further simplified,

$$H = I_1 + \overline{\nu} I_2 - \alpha \left( \sum_i r_{E_i} \right) \sin\theta, \tag{19}$$

which has the same form of the Hamiltonian used in Refs. [1,2], with an effective $\alpha$,

$$\alpha_{eff} = \alpha \sum_i r_{E_i}. \tag{20}$$

Therefore we can conclude that for $\Delta\theta \ll 1$, in the case of coherent waves, the threshold for the onset of stochastic diffusion is reduced in the case of several waves, as compared to the one-wave case. Particularly, if all waves have the same amplitude, using condition (8) we obtain

$$\alpha_{eff} = \alpha (n_\omega)^{1/2}. \tag{21}$$

This result shows that the increase in the number of coherent waves, even with amplitudes restricted by the condition $\langle E^2 \rangle = E_0^2$, decreases the threshold for the occurrence of stochastic diffusion, since the value of $\alpha$ necessary to produce the same effect caused with one wave is decreased by the factor $\Sigma_i r_{E_i}$. In the limiting case of a continuous spectrum of coherent waves, with an infinite number of waves, this result predicts that the threshold goes to zero and that the initial diffusion occurs even for vanishing value of $\alpha$.

After the initial stages, the subsequent evolution is no longer ruled by Eq. (19), but rather by Eq. (15), or Eq. (13). The behavior of the system in that case, as well in the more general case of incoherent waves, must therefore be the object of a numerical analysis, with results presented in Sec. III.

## III. SOME NUMERICAL RESULTS

For the numerical solution of the Hamiltonian equations, we assume a given number of particles ($n_p$) and a given number of waves ($n_\omega$) and give $\alpha$ and $\overline{\nu}$ as parameters. We also assume a given value of $\Delta$ and a distribution of wave amplitudes $r_{E_i}$.

As loading procedure for the numerical calculation, we initially consider the following case: We give parameters $I_1^0$, $a_0$, and the initial Hamiltonian $H$, and attribute, for the $n_p$ particles, regularly spaced values of $I_1$, $\omega_1$, and $\omega_2$:

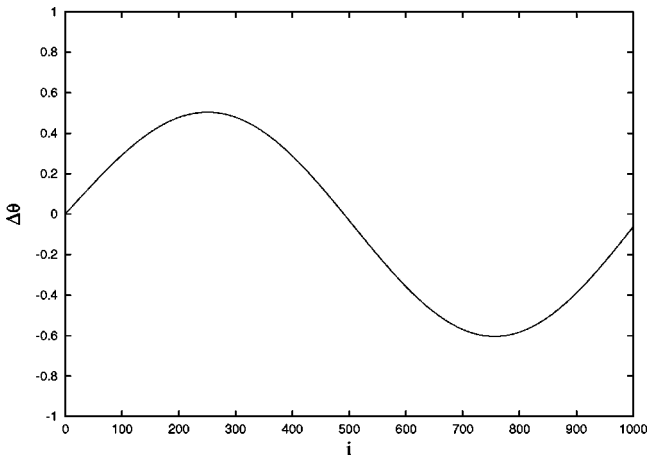


FIG. 1. Initial values of $\Delta\theta$ vs particle index $i$, for $n_p=1000$ particles, assuming $I_1=1.25\times10^3$, $a_0=400$, and $\Delta=1.0\times10^{-2}$. The initial conditions for the particles are attributed such that $\omega_1$ and $\omega_2$ are between 0 and $2\pi$ and $I_1$ is between $I_1^0$ and $I_1^0+a_0$, and $I_2$ is evaluated under the restriction that all particles have the same value of the Hamiltonian ($H$).

$$I_1=I_1^0+\frac{1}{n_p}a_0, I_1^0+\frac{2}{n_p}a_0, \ldots, I_1^0+a_0,$$

$$\omega_1=2\pi\frac{1}{n_p}, 2\pi\frac{2}{n_p}, \ldots, 2\pi,$$

$$\omega_2=2\pi\frac{1}{n_p}, 2\pi\frac{2}{n_p}, \ldots, 2\pi,$$

$$I_2=(H-I_1+S)/\overline{\nu}, \tag{22}$$

where

$$S\equiv\alpha\sum_i\frac{r_{E_i}}{r_{\omega_i}}\sin\{r_{\omega_i}[R\sin(\omega_1)-\omega_2]-\phi_i\}.$$

In other words, the loading procedure assumes initial values for $I_1$, $\omega_1$, and $\omega_2$, and evaluates $I_2$ in such a way that all the particles have the same initial Hamiltonian ($H$), for which we have arbitrarily assumed the value $H=I_1^0+\overline{\nu}I_1^0$. Once we know the initial values of $\omega_1$, $\omega_2$, $I_1$, and $I_2$, it is possible to evaluate the value of the product $\Delta\theta$.

When assuming the initial value of $I_1$ for each particle, we are simply assuming the initial value of the perpendicular canonical momentum of the particles, since reversing the canonical transformations one obtains

$$I_1=\frac{1}{2}\frac{\overline{k^2}}{m^2\Omega^2}[p_y^2+(p_x-qA_x)^2],$$

where $p_x$ and $p_y$ are the $x$- and $y$-dimensional components of the particle momentum, as used in Eq. (3), before the introduction of the dimensionless variables by Eq. (4).

In Fig. 1 we show the initial value of $\Delta\theta$ for $n_p=1000$ particles, assuming $I_1=1.25\times10^3$, $a_0=400$, and $\Delta=1.0\times10^{-2}$. It is seen that the quantity $\Delta\theta$ is indeed smaller than unity for all particles, which means that the Hamiltonian equation as given by Eq. (18) approximately rules the initial stages of the evolution of the system, in the particular case of coherent waves.

With this choice of parameters $I_1^0$ and $a_0$, the spread of perpendicular momenta of the particles is such that $50.0<R<57.4$, where, as we have seen, $R=\sqrt{2I_1}$. Assuming for instance $\overline{\nu}=30$ and vanishing wave intensity ($\alpha=0$), the quantity $\sqrt{2I_2}$ therefore satisfies $49.7<\sqrt{2I_2}<50.0$, having limits slightly different from these values in the case of finite $\alpha$, according to Eq. (22). This range of parameters is similar to that utilized in previous studies of the one-wave case, which we use for comparison when considering the case of several waves [1,2].

According to these studies, for one wave and integer value of $\overline{\nu}$, and small wave amplitude, the phase space is dominated by large first-order islands. At intermediate wave amplitudes, stochastic motion appears near the separatrixes between the islands. For growing wave amplitude the size of the stochastic region increases, and the threshold for stochasticity has been defined as the wave amplitude for which the fraction of phase space occupied by the islands has appreciably diminished in comparison with the size of stochastic regions [1]. The limits of the stochastic region are $\alpha$ dependent and have been established approximately as the following [1]:

$$R_{min}=\overline{\nu}-\sqrt{\alpha}, \quad R_{max}=(4\alpha\overline{\nu})^{2/3}(2/\pi)^{1/3}.$$

For $\alpha=2.0$, the stochasticity therefore will fully occur in the region $28.6<R<33.2$. For $\alpha=4.0$, in the region $28.0<R<43.5$, and for $\alpha=6.0$, in the region $27.5<R<69.0$. Therefore, for our choice of parameters, in the one-wave case we may expect a small amount of stochasticity for $\alpha=2.0$, for instance, since the range $50.0<R<57.4$ is far from the stochastic range, and an appreciable amount of stochasticity for $\alpha=4.0$, since the range $50.0<R<57.4$ is close to the stochastic range. On the other hand, for a larger wave amplitude, as in the case of $\alpha=6.0$, for instance, one can expect fully established stochasticity in the chosen range, which will be completely immersed in the stochastic region.

### A. The one-wave case

We start by considering the one-wave case, the situation considered in Refs. [1] and [2].

In order to illustrate the effect of the increase of the wave intensity, we present in Fig. 2 the quantity $\sqrt{2I_2}$ vs $\omega_2 \pmod{2\pi}$, for the case of three particles and one wave, with $\alpha=2.2$, 3.0, 3.8, and 4.6, assuming $I_1^0=1.25\times10^3$, $a_0=400$, and $\overline{\nu}=30.0$. The sequence of panels illustrates the gradual modification of particle trajectories caused by the increase in the wave intensity. In Fig. 3 we present the same quantity $\sqrt{2I_2}$ vs $\omega_2 \pmod{2\pi}$, for the case of 50 particles and $\alpha=2.0$, using the same parameters and initial conditions as for Fig. 2. We see the gradual appearance of the overlap of particle orbits which has been shown to correspond to stochastic diffusion in velocity space [1,2].

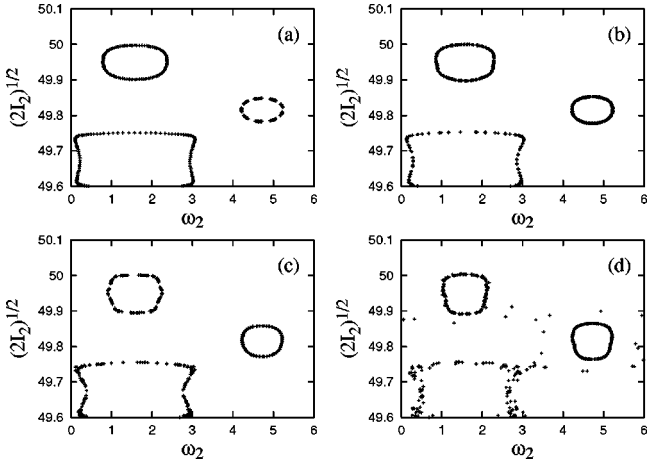


FIG. 2. $\sqrt{2I_2}$ as a function of $\omega_2(\mathrm{mod}\,2\pi)$ for three particles, one wave, $\bar{\nu}=30$, and (a) $\alpha=2.2$, (b) $\alpha=3.0$, (c) $\alpha=3.8$, and (d) $\alpha=4.6$.

### B. The case of several waves with the same phase

We now consider the presence of more than one wave, with different frequencies, all with the same phase factor of the central wave ($\bar{\phi}=0$). For simplicity, we assume that all waves have the same amplitude such that $r_E=(n_\omega)^{-1/2}$. This simple limiting case displays some of the effects due to the increase in the number of waves, to be compared with the more general case of a set of incoherent waves discussed at the end of the present section.

For instance, Fig. 4 shows the case of $\sqrt{2I_2}$ vs $\omega_2(\mathrm{mod}\,2\pi)$, considering three particles and $\alpha=2.0$ for several values of the number of waves (1, 3, 5, and 7), using $\Delta=1.0\times10^{-2}$ and the same parameters and initial conditions as for Fig. 2. It is seen that the increase in the number of waves produces modifications in the particle trajectories which are reminiscent of the modifications caused by the increase in the wave intensity, shown in Fig. 2.

The effect of the increase in the number of coherent waves on a larger number of particles is seen in Fig. 5, where

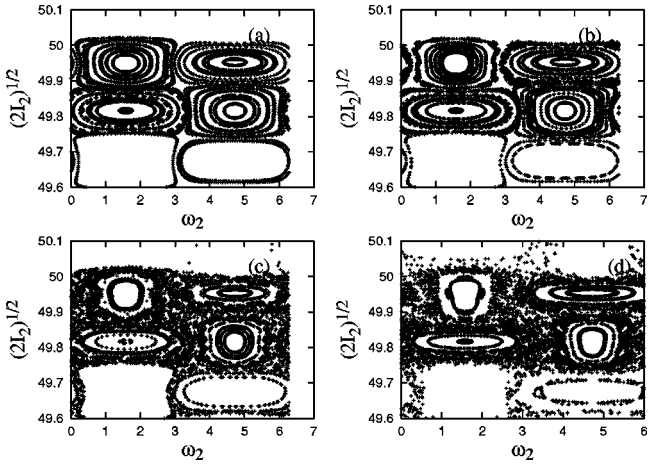


FIG. 3. $\sqrt{2I_2}$ as a function of $\omega_2(\mathrm{mod}\,2\pi)$, for 50 particles, one wave, $\bar{\nu}=30$, and (a) $\alpha=2.2$, (b) $\alpha=3.0$, (c) $\alpha=3.8$, and (d) $\alpha=4.6$.

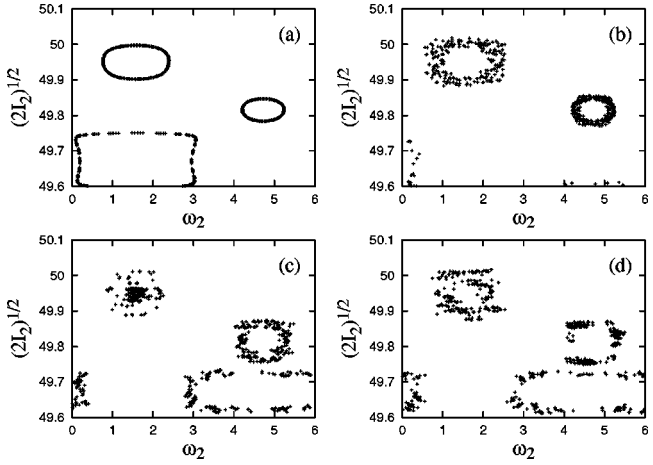


FIG. 4. $\sqrt{2I_2}$ as a function of $\omega_2(\mathrm{mod}\,2\pi)$ for three particles and coherent waves, $\alpha=2.0$, $\bar{\nu}=30$, $\Delta=1.0\times10^{-2}$, and number of waves (a) 1, (b) 3, (c) 5, and (d) 7.

we present $\sqrt{2I_2}$ vs $\omega_2(\mathrm{mod}\,2\pi)$ for the case of 50 particles and $\alpha=2.0$, for several values of the number of waves (1, 3, 5, and 7). In this figure, we also use the same parameters and initial conditions used to obtain Fig. 4.

Looking for more information on the behavior of the system, we consider in Fig. 6 the case in which five waves are present in the system, considering several values of the wave amplitude ($\alpha=0.25$, 0.5, 1.0, and 2.0), and $\Delta=1.0\times10^{-2}$. As in previous figures, Fig. 6 depicts $\sqrt{2I_2}$ as a function of $\omega_2(\mathrm{mod}\,2\pi)$. The loading procedure and other parameters are also the same as in previous figures. It has confirmed the expectation that the presence of more than one wave is not sufficient to guarantee the occurrence of stochastic diffusion, but the threshold of wave intensity for the onset of stochasticity is reduced as compared to the one-wave case, which occurs for $\alpha\simeq2.2$. Visually, this onset appears to occur between the case of $\alpha=0.5$, where the particle orbits obtained are similar to those appearing in the first panel of Fig. 5 (one wave case with $\alpha=2.0$), and the case of $\alpha$

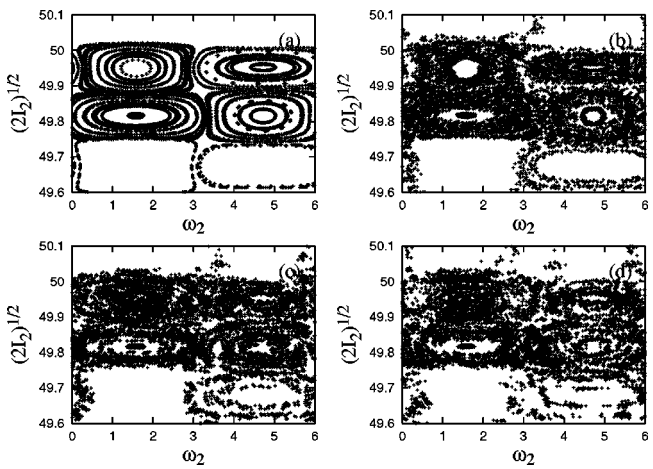


FIG. 5. $\sqrt{2I_2}$ as a function of $\omega_2(\mathrm{mod}\,2\pi)$ for 50 particles and coherent waves, $\alpha=2.0$, $\Delta=1.0\times10^{-2}$, and number of waves (a) 1, (b) 3, (c) 5, and (d) 7.

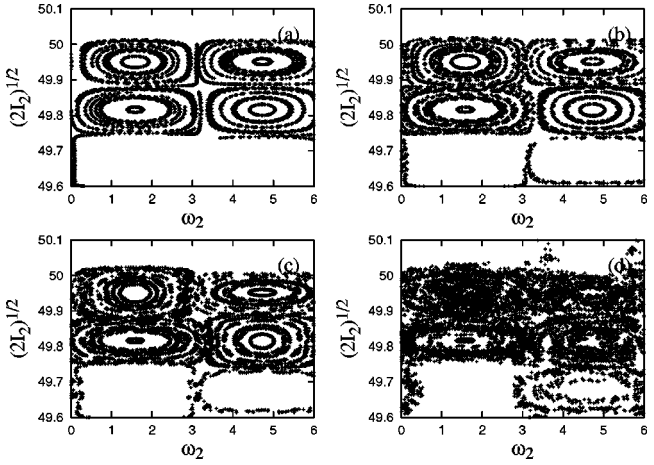


FIG. 6. $\sqrt{2I_2}$ as a function of $\omega_2(\mathrm{mod}\,2\pi)$ for 50 particles and coherent waves, $\Delta=1.0\times10^{-2}$, $n_\omega=5$, and (a) $\alpha=0.25$, (b) $\alpha=0.5$, (c) $\alpha=1.0$, and (d) $\alpha=2.0$.

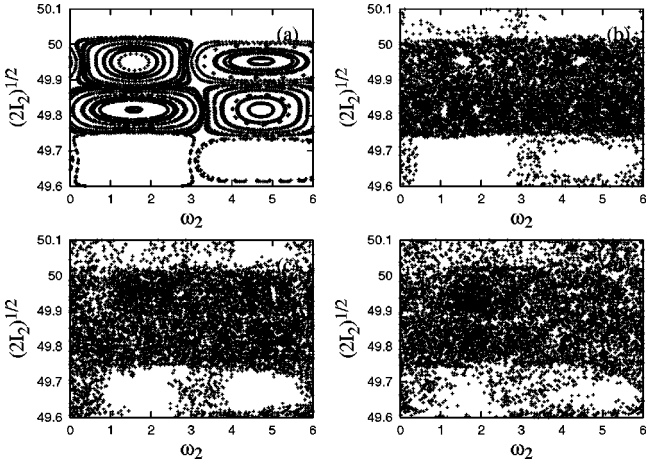


FIG. 8. $\sqrt{2I_2}$ as a function of $\omega_2(\mathrm{mod}\,2\pi)$, for 50 particles and waves with random phases, $\alpha=2.0$, $\Delta=1.0\times10^{-2}$, and number of waves (a) 1, (b) 3, (c) 5, and (d) 7.

$=1.0$. This is in agreement with Eq. (21), which predicts $\alpha=\alpha_{1wave}/(n_\omega)^{1/2}$ (which in the present case is $2.2/(5)^{1/2}\simeq0.98$).

### C. The case of several waves with random phases

We now consider the presence of more than one wave, with different frequencies and random phases, with the phase of the central wave assumed to be zero ($\bar{\phi}=0$). The random phases are obtained from a random number generator that starts from a numerical seed. All the results that follow, unless explicitly stated otherwise, are generated using same seed for the random number generator. Regarding the amplitudes in the set of waves, we assume that they are all equal, such that $r_E=(n_\omega)^{-1/2}$.

For instance, Fig. 7 shows the case of $\sqrt{2I_2}$ vs $\omega_2(\mathrm{mod}\,2\pi)$, considering three particles and $\alpha=2.0$, for several values of the number of waves (1, 3, 5, and 7), using $\Delta=1.0\times10^{-2}$ and the other parameters as in Fig. 2. Except for the random phases, these are exactly the same conditions used to generate Fig. 4. The modifications in the particle trajectories are similar but more impressive than those caused by coherent waves, seen in Fig. 4.

The effect of the increase in the number of incoherent waves on a larger number of particles is seen in Fig. 8, where we present $\sqrt{2I_2}$ vs $\omega_2(\mathrm{mod}\,2\pi)$ for the case of 50 particles and $\alpha=2.0$, for several values of the number of waves (1, 3, 5, and 7). In this figure, we also use the same parameters used to obtain Fig. 7. Figure 8 clearly shows that the presence of the waves with random phases causes the complete spreading of the particle orbits that are present in the case of only one wave, for the same value of $\alpha$.

As in the case of coherent waves, with results shown in Fig. 6, in Fig. 9 we show $\sqrt{2I_2}$ as a function of $\omega_2(\mathrm{mod}\,2\pi)$ for the case in which five waves are present in the system, considering several values of the wave amplitude ($\alpha=0.25$, 0.5, 1.0, and 2.0), and $\Delta=1.0\times10^{-2}$, and waves with random phases. The loading procedure and other pa-

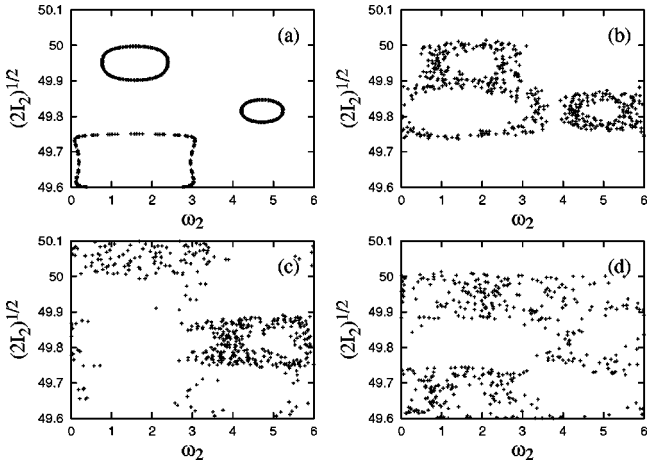


FIG. 7. $\sqrt{2I_2}$ as a function of $\omega_2(\mathrm{mod}\,2\pi)$ for three particles and waves with random phases, $\alpha=2.0$, $\bar{\nu}=30$, $\Delta=1.0\times10^{-2}$, and number of waves (a) 1, (b) 3, (c) 5, and (d) 7.

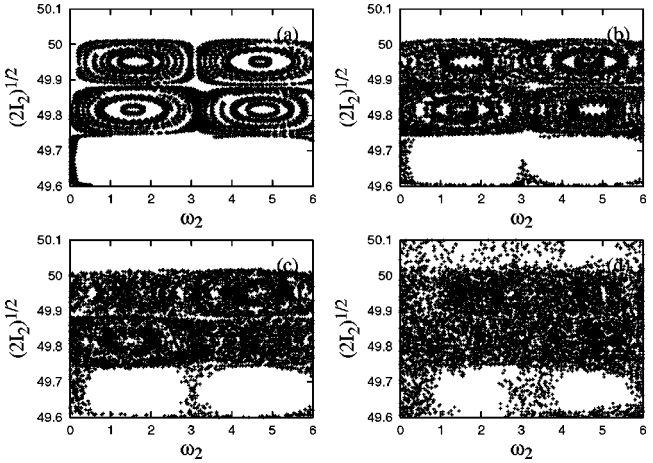


FIG. 9. $\sqrt{2I_2}$ as a function of $\omega_2(\mathrm{mod}\,2\pi)$ for 50 particles and waves with random phases, $\Delta=1.0\times10^{-2}$, $n_\omega=5$, and (a) $\alpha=0.25$, (b) $\alpha=0.5$, (c) $\alpha=1.0$, and (d) $\alpha=2.0$.

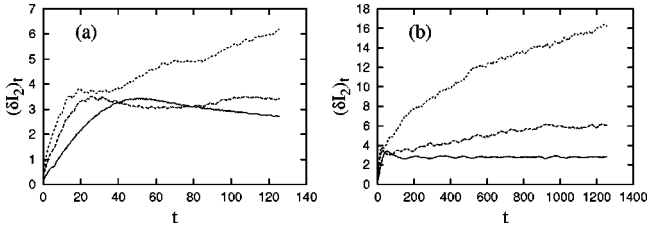


FIG. 10. $(\delta I_2)_t$ as a function of normalized time for $n_\omega=1$, $I_1^0=1.25\times10^3$, $a_0=400$, $\overline{\nu}=30.0$, and $\alpha=2.0$ (full line), 4.0 (broken line), and 6.0 (dotted line). (a) Short-term evolution; (b) long-term evolution.

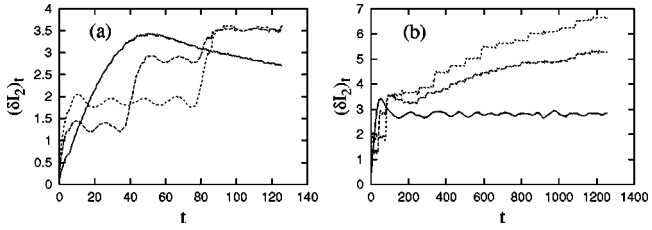


FIG. 11. $(\delta I_2)_t$ as a function of normalized time for the case of coherent waves, for $I_1^0=1.25\times10^3$, $a_0=400$, $\overline{\nu}=30.0$, and $\alpha=2.0$, for $n_\omega=1$ (full line), 5 (broken line), and 9 (dotted line). (a) Short-term evolution; (b) long-term evolution.

rameters are also the same as in previous figures. We observe that the amount of stochastic diffusion, for the same number of iterations, gradually decreases when the wave energy is reduced, but even in the case of $\alpha=0.25$ the degree of stochasticity is larger than that obtained in the one-wave case and $\alpha=2.0$, as seen in the first panel of Fig. 5 and in the first panel of Fig. 8. However, while in the case of coherent waves we can use Eq. (21) in order to relate the amplitude required for the onset of stochasticity with the amplitude required to produce a similar effect in the one-wave case, we have not developed an equivalent theoretical approach for the case of waves with random phases.

Figure 9(a) also shows a higher degree of stochasticity than Fig. 6(a), with the only difference being that Fig. 9(a) was obtained assuming waves with random phases, while Fig. 6(a) was obtained assuming all waves possess the same phase ($\phi=0$). In the analysis that appears in the following section, we will similarly observe more pronounced long-term diffusive behavior in the case of waves with random phases than in the case of waves with the same phase. subsection

### D. Comparative analysis of the one-wave case and the cases with several waves, coherent and incoherent

The presence of stochastic behavior can also be investigated by following the time behavior of the following quantities:

$$(\delta I_j)_t=\left\{\frac{1}{n_p-1}\sum_{i=1}^{n_p}[I_j(t)-I_j(0)]^2\right\}^{1/2}, \qquad (23)$$

where $j=1,2$. In a plot of $(\delta I_j)_t$ vs $t$, the inclination of $(\delta I_j)_t$ relative to the $t$ axis is a measure of the diffusion coefficient in velocity space [11].

In Fig. 10 we show $(\delta I_2)_t$ as a function of normalized time for the one-wave case ($n_\omega=1$), $I_1^0=1.25\times10^3$, $a_0=400$, $\overline{\nu}=30.0$, and $\alpha=2.0$, 4.0, and 6.0. Panel (a) of Fig. 10 shows the evolution up to normalized $t\simeq120$, and panel (b) shows the extended evolution, up to $t\simeq1200$. For this figure, we have considered $n_p=1000$, which results in much better statistics than obtained with $n_p=50$. The Poincaré plots presented in Figs. 2–8, on the other hand, were obtained with $n_p=50$ because with a larger number of particles it becomes very difficult to see any structure in the plots, due to the proximity of the dots that represent successive passages of particles by the Poincaré section. Figure 10 clearly shows that long-term diffusive behavior, measured by the inclination of the curve relative to the $t$ axis, is absent in the case of $\alpha=2.0$ but is already present in the case of $\alpha=4.0$, and is more impressive in the case of $\alpha=6.0$ [1,2].

In Fig. 11 we show $(\delta I_2)_t$ as a function of normalized time for $I_1^0=1.25\times10^3$, $a_0=400$, $\overline{\nu}=30.0$, and $\alpha=2.0$, for $n_\omega=1$, 5, and 9, for the case of coherent waves. Panel (a) shows the evolution up to $t\simeq120$, while panel (b) shows the evolution up to $t\simeq1200$. Figure 11 also shows the progressive appearing of diffusion in the system, but the curves that display the growth of $(\delta I_2)_t$ with time exhibit smaller average inclination than in the case corresponding to one wave and $\alpha=2.0$, appearing in Fig. 10. It is also noticeable the alternance of regions where the curve describing $(\delta I_2)_t$ grows with time and regions where it is nearly constant and parallel to the horizontal axis. This sequence of steps is not noticeable in the one-wave case in Fig. 10.

In Fig. 12 we show $(\delta I_2)_t$ as a function of normalized time for $I_1^0=1.25\times10^3$, $a_0=400$, $\overline{\nu}=30.0$, and $\alpha=2.0$, for $n_\omega=1$, 5, and 9, for the case of waves with random phases. As in Fig. 11, panel (a) shows the evolution up to $t\simeq120$, while panel (b) shows the evolution up to $t\simeq1200$. According to Fig. 12, the initial evolution of $(\delta I_2)_t$ displays smaller inclination toward the $t$ axis than in the corresponding cases for coherent waves appearing in Fig. 11. But the long-term evolution appearing in Fig. 12(b) shows continued diffusion, without the conspicuous ''steps'' appearing in Fig. 11, in the case of coherent waves, resulting that the quantity $(\delta I_j)_t$ attains larger values in the case of Fig. 12(b) than in the case appearing in Fig. 11(b). Another interesting feature appearing in Fig. 12(b) is that the cases of $n_{wave}=5$ and $n_{wave}=9$ with

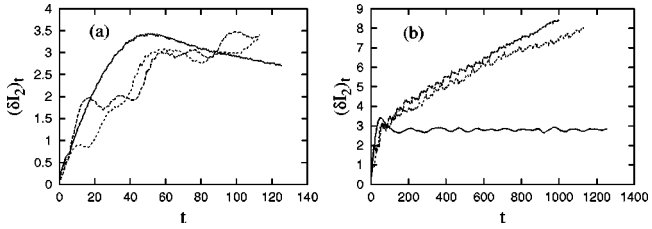


FIG. 12. $(\delta I_2)_t$ as a function of normalized time for the case of waves with random phases, for $I_1^0=1.25\times10^3$, $a_0=400$, $\overline{\nu}=30.0$, and $\alpha=2.0$, for $n_\omega=1$ (full line), 5 (broken line), and 9 (dotted line). (a) Short-term evolution; (b) long-term evolution.

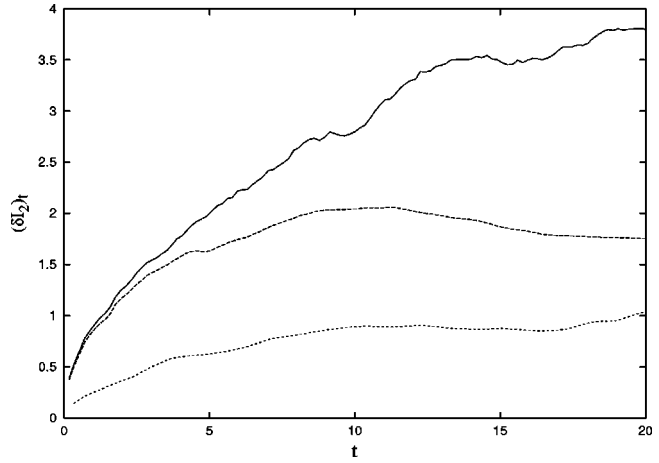


FIG. 13. Early stages of the evolution of $(\delta I_2)_t$ as a function of normalized time for $n_\omega=1$ and $\alpha=6.0$ (full line), for $n_\omega=9$ and $\alpha=2.0$, coherent waves (broken line), and for $n_\omega=9$ and $\alpha=2.0$, waves with random phases (dotted line), assuming $I_1^0=1.25\times10^3$, $a_0=400$, and $\overline{\nu}=30.0$.

random phases exhibit similar long-term behavior of $(\delta I_2)_t$, different from the behavior appearing in Fig. 11 for the case of coherent waves.

The very early stages of the time evolution are shown in Fig. 13 that displays $(\delta I_2)_t$ vs normalized time for the cases $n_\omega=1$ and $\alpha=6.0$, $n_\omega=9$ and $\alpha=2.0$ for coherent waves, and $n_\omega=9$ and $\alpha=2.0$ for waves with random phases, assuming $I_1^0=1.25\times10^3$, $a_0=400$, and $\overline{\nu}=30.0$, and $t$ up to 20. According to Eqs. (21), the two former cases should feature similar initial diffusion rates, a prediction which is corroborated by the results shown in Fig. 13. Regarding the results featured in the case of random waves, at least for the set of random phases utilized, the early inclination of the curve for $(\delta I_2)_t$ is smaller than in the case of the set of coherent waves, although we observe continued and more significant diffusion for long-time evolution according to the comparison between Figs. 11 and 12.

The results shown in Figs. 10, 11, and 13 show that the stochastic diffusion caused for several coherent waves indeed starts at the wave level predicted by using Eq. (21), but proceeds at a smaller average pace than the corresponding case with only one wave. These results can be understood by considering some features of the equations of motion. Let us consider, for instance, the fourth equation of motion appearing in Eqs. (16) and (17), averaged for all particles,

$$\xi_2 \equiv \frac{1}{n_p}\sum_{j=1}^{n_p}\dot{I}_2 = -\frac{1}{n_p}\sum_{j=1}^{n_p}\sum_i r_{E_i}[\cos(i\Delta'\theta)\cos(\theta-\phi_i) - \sin(i\Delta'\theta)\sin(\theta-\phi_i)], \tag{24}$$

which can be taken as representative of the behavior of the system. In Fig. 14 we plot $\xi_2$ vs normalized time for $\alpha=2.0$ and $n_\omega=1$, 5, and 9, assuming coherent waves, $I_1^0=1.25\times10^3$, $a_0=400$, and $\overline{\nu}=30.0$. The curves appearing in the left three panels of Fig. 14 should be compared with

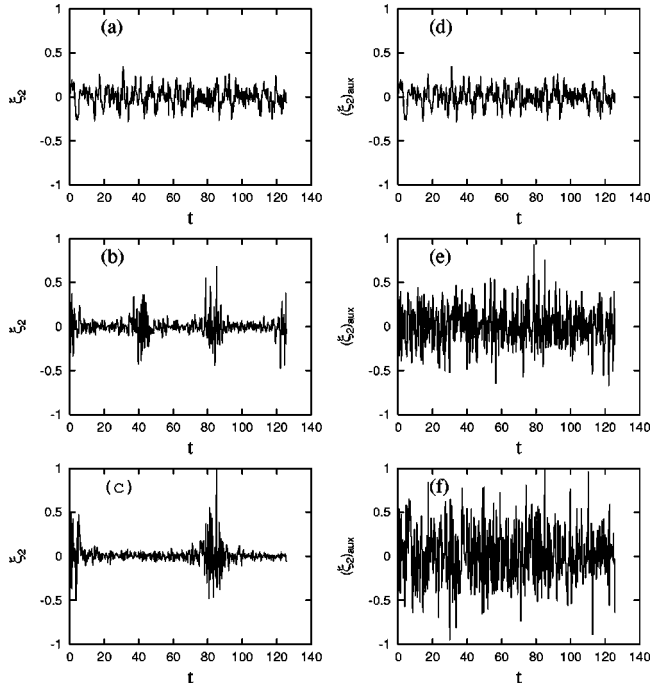


FIG. 14. Left panels: the quantity $\xi_2$ as a function of normalized time, in the case of coherent waves, for $\alpha=2.0$ and (a) $n_\omega=1$, (b) $n_\omega=5$, and (c) $n_\omega=9$, assuming $I_1^0=1.25\times10^3$, $a_0=400$, and $\overline{\nu}=30.0$. Right panels: the quantity $[\xi_2]_{\rm aux}$ as a function of normalized time for the same parameters as in the left panels. (d) $n_\omega=1$, (e) $n_\omega=5$, and (f) $n_\omega=9$.

the curves appearing in the corresponding right panels of Fig. 14, where we plot the auxiliary quantity

$$(\xi_2)_{\rm aux} \equiv -\frac{1}{n_p}\sum_{j=1}^{n_p}\alpha\left[\sum_i r_{E_i}\right]\cos(\theta), \tag{25}$$

which is simply the average of the equation of motion that would rule the evolution of $I_2$ if $\Delta\theta$ could be considered very small along all the time interval shown in the figure. In that case, the stochasticity would occur as in the one-wave case, with $\alpha_{eff}=\alpha\Sigma_i r_{E_i}$.

The comparison between the corresponding left and right panels of Figs. 14 shows that the quantity $[\xi_2]_{\rm aux}$ is a fluctuating quantity with a significant amplitude along the time evolution, while $\xi_2$ for coherent waves is a fluctuating quantity that in the case of $n_p>1$ features a much smaller amplitude along most of the time span considered in the calculations, with periodic bursts of amplitude. The modulation of the time evolution of the quantity $\xi_2$, which occurs due to the factors $\cos(i\Delta'\theta)$ appearing in the equation of motion, explains the smaller amount of diffusion in velocity space when compared with the diffusion that would occur without the presence of the modulation, for the same parameters.

The maxima of the quantity $\xi_2$, which appear periodically in Fig. 14, may be easily explained as follows. The periodicity originates from the factor $\Sigma_i r_{E_i}\cos(i\Delta'\theta)$, which in the case of equal amplitude waves may be written as

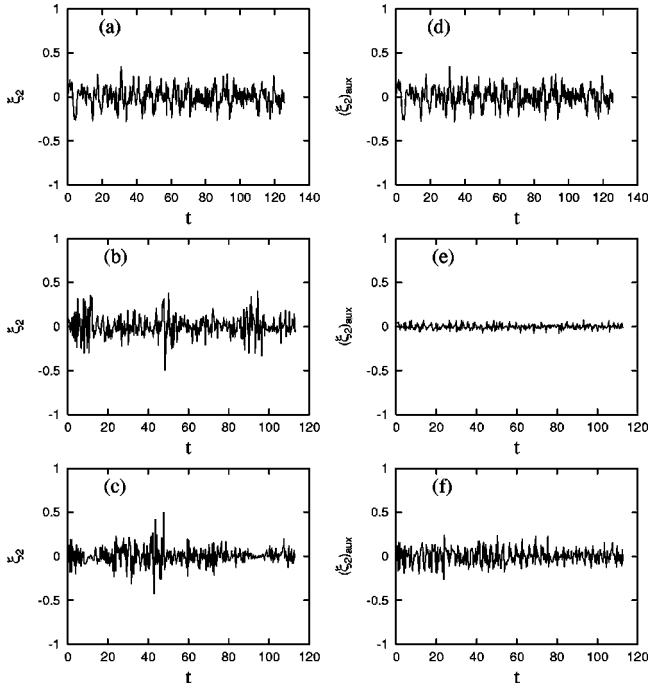


FIG. 15. Left panels: the quantity $\xi_2$ as a function of normalized time, in the case of waves with random phases, for $\alpha=2.0$ and (a) $n_\omega=1$, (b) $n_\omega=5$, and (c) $n_\omega=9$, assuming $I_1^0=1.25\times10^3$, $a_0=400$, and $\overline{\nu}=30.0$. Right panels: the quantity $[\xi_2]_{\rm aux}$ as a function of normalized time for the same parameters as in the left panels. (d) $n_\omega=1$, (e) $n_\omega=5$, and (f) $n_\omega=9$.

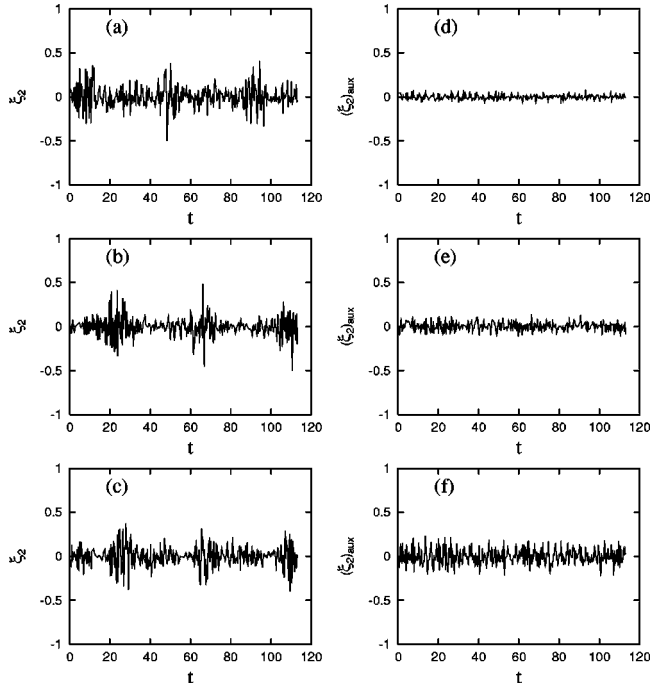


FIG. 16. Left panels: the quantity $\xi_2$ as a function of normalized time, in the case of waves with random phases, for $n_\omega=5$ and $\alpha=2.0$, with three different sets of random phases, obtained with different seeds for the numerical evaluation of the phases, assuming $I_1^0=1.25\times10^3$, $a_0=400$, and $\overline{\nu}=30.0$. Right panels: the quantity $[\xi_2]_{\rm aux}$ as a function of normalized time for the same parameters as in the left panels.

$$\sum_{i=-n_i}^{n_i} r_{E_i}\cos(i\Delta'\theta)=r_{E_0}\sum_{i=-n_i}^{n_i}\cos(i\Delta'\theta)$$

$$=r_{E_0}\frac{\sin\left(\dfrac{n_\omega\Delta\theta}{n_\omega-1}\right)}{\sin\left(\dfrac{\Delta\theta}{n_\omega-1}\right)}.$$

The maxima of this quantity for $n_\omega>1$ are located at $|\theta|=(k\pi/\Delta)(n_\omega-1)$, where $k$ is a positive integer. Since $\theta$ averaged for all particles is $\theta\simeq-\overline{\nu}t$, that means that the maxima occur at $t\simeq k\pi(n_\omega-1)/(\overline{\nu}\Delta)$. For our parameters, the first maxima therefore occurs for $t\simeq40$ and $t\simeq80$, respectively, for $n_\omega=5$ and 9. The following maxima occur at multiples of these values. These features are seen in Fig. 14 and explain the sequence of diffusive steps exhibited in Fig. 11. A consequence of this bursty diffusive behavior is that, although the threshold for the onset of stochastic diffusion is decreased by the presence of a set of coherent waves with close frequencies, if compared to the one-wave case, as predicted by Eq. (21), the overall diffusion is limited by the time interval between the diffusive episodes, which becomes increasingly large with the increase in the number of waves.

In Fig. 15, on the other hand, we plot $\xi_2$ vs normalized time for $\alpha=2.0$ and $n_\omega=1$, 5, and 9, assuming waves with random phases, $I_1^0=1.25\times10^3$, $a_0=400$, and $\overline{\nu}=30.0$. As in the case of Fig. 14, the curves appearing in the left three panels of Fig. 15 should be compared with the curves appearing in the corresponding right panels of Fig. 15, where the auxiliary quantity $[\xi_2]_{\rm aux}$ is plotted as a function of normalized time.

The comparison between the corresponding left and right panels of Figs. 15 shows that the quantity $[\xi_2]_{\rm aux}$ is a fluctuating quantity whose amplitude along the time evolution depends on the phase of the waves composing the wave packet in the **k** space. For the seed used in the generation of the random phases, we observe that the amplitude of $[\xi_2]_{\rm aux}$ in the case of $n_{wave}=5$ is smaller than in the case of $n_{wave}=1$ or 9, while $\xi_2$ is a fluctuating quantity that does not show the regular appearance of maxima and minima that we have seen in Fig. 14, in the case of coherent waves. The absence of that regular modulation in the case of waves with random phases explains the absence of the diffusive steps that occurs for coherent waves, and explains the relatively regular and continued diffusion caused for waves with random phases as seen in Fig. 12(b).

The influence of the random phases in the case of a finite number of waves is illustrated in Fig. 16, which shows the quantities $\xi_2$ and $[\xi_2]_{\rm aux}$ for the case of $n_{wave}=5$, with other parameters as in Fig. 15, and three different sets of random phases, generated with three different numerical seeds for the random number generator. Panel (a) of Fig. 16 corresponds to the case of panel (b) of Fig. 15. The right hand panels show different amplitudes for the quantity $[\xi_2]_{\rm aux}$, which illustrate the dependence on the phases. The left hand panels,

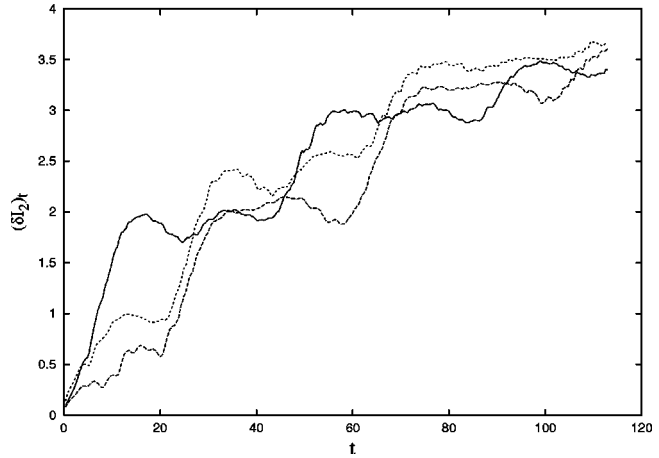


FIG. 17. Short-term evolution of $(\delta I_2)_t$ as a function of normalized time, in the case of waves with random phases, for $n_\omega = 5$ and $\alpha = 2.0$, with three different sets of random phases, obtained with different seeds for the numerical evaluation of the phases, assuming $I_1^0 = 1.25 \times 10^3$, $a_0 = 400$, and $\overline{\nu} = 30.0$.

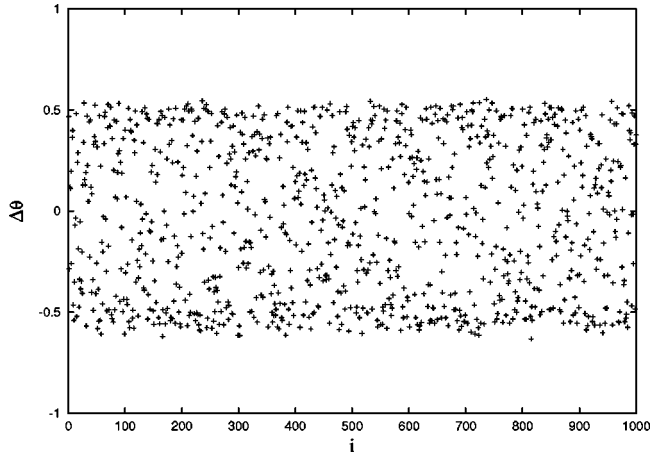


FIG. 18. Initial values of $\Delta\theta$ vs particle index $i$ for $n_p = 1000$ particles, assuming $I_1 = 1.25 \times 10^3$, $a_0 = 400$, and $\Delta = 1.0 \times 10^{-2}$. The initial conditions for the particles are randomly attributed, such that $\omega_1$ and $\omega_2$ are between 0 and $2\pi$ and $I_1$ is between $I_1^0$ and $I_1^0 + a_0$, with $I_2$ evaluated under the restriction that all particles have the same value of the Hamiltonian ($H$).

on the other hand, exhibit the difference but have in common the irregular appearance of maxima and minima of similar amplitudes in all three cases shown. As a consequence, the diffusive behavior caused by the waves is roughly similar for the three cases, as shown in Fig. 17, which displays the short-term behavior of $(\delta I_2)_t$, for the three cases of different sets of random phases used to obtain Fig. 16. In spite of the obvious differences between the three curves obtained, the inclination relative to the $t$ axis is approximately the same in the three cases, indicating similar average diffusive behavior. A more exhaustive investigation would require very intensive use of numerical calculations, considering a large number of sets of random phases, which we believe will not bring any significant modification to the general trend exposed in Fig. 17. It is expected that the average behavior obtained with different sets of random phases would tend to become more and more similar for increasing number of waves, so that in the limit of infinite wave number the diffusion caused by the waves would be independent of the particular set of random phases utilized in the calculation.

### E. An example with different initial conditions

The regularity of the initial conditions utilized for the particles to obtain the results presented up to this point in the present section has been useful in order to generate regular Poincaré plots as those appearing for instance in Figs. 3(a), 5(a), and 8(a). However, it is necessary to investigate whether results similar to those obtained up to this point may be found also under different initial conditions or whether they are peculiar to the conditions assumed at the beginning of the section. We therefore consider here another example, which assumes for the particles $I_1$ values randomly distributed between $I_1^0$ and $I_1^0 + a_0$, and $\omega_1$ and $\omega_2$ values randomly distributed between 0 and $2\pi$, with the quantity $I_2$ evaluated according to Eq. (22), under the condition that the Hamiltonian value ($H$) is the same for all particles.

The randomness of the initial conditions in this case can be appreciated in Fig. 18, where we show the initial value of $\Delta\theta$ for $n_p = 1000$ particles, assuming $I_1 = 1.25 \times 10^3$, $a_0 = 400$, and $\Delta = 1.0 \times 10^{-2}$. As in Fig. 1, it is seen that the quantity $\Delta\theta$ is indeed smaller than unity for all particles.

In Fig. 19 we present for these initial conditions the quantity $(\delta I_2)_t$ as a function of normalized time for the one-wave case ($n_\omega = 1$), $I_1^0 = 1.25 \times 10^3$, $a_0 = 400$, $\overline{\nu} = 30.0$, and $\alpha = 2.0$, 4.0, and 6.0, considering $n_p = 1000$. Panel (a) of Fig. 19 shows the evolution up to normalized $t \simeq 120$, and panel (b) shows the extended evolution, up to $t \simeq 1200$. Similarly to what we obtained in Fig. 10 for the case of the more regular set of initial conditions, Fig. 19 clearly shows that long-term diffusive behavior is absent in the case of $\alpha = 2.0$, but is already present in the case of $\alpha = 4.0$, and is more impressive in the case of $\alpha = 6.0$ [1,2].

In Fig. 20, we show $(\delta I_2)_t$ as a function of normalized time for $I_1^0 = 1.25 \times 10^3$, $a_0 = 400$, $\overline{\nu} = 30.0$, and $\alpha = 2.0$, for $n_\omega = 1$, 5, and 9, for the case of coherent waves. Panel (a) shows the evolution up to $t \simeq 120$, while panel (b) shows the

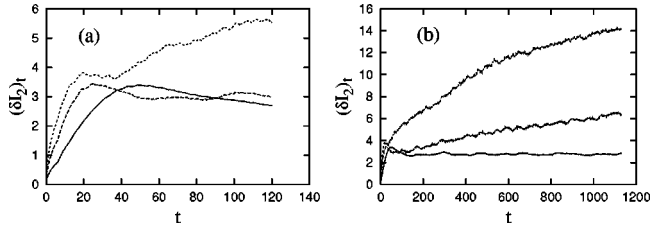


FIG. 19. $(\delta I_2)_t$ as a function of normalized time for $n_\omega = 1$, $I_1^0 = 1.25 \times 10^3$, $a_0 = 400$, $\overline{\nu} = 30.0$, and $\alpha = 2.0$ (full line), 4.0 (broken line), and 6.0 (dotted line). (a) Short-term evolution; (b) long-term evolution. The initial conditions for the particles are randomly attributed, such that $\omega_1$ and $\omega_2$ are between 0 and $2\pi$ and $I_1$ is between $I_1^0$ and $I_1^0 + a_0$, with $I_2$ evaluated under the restriction that all particles have the same value of the Hamiltonian ($H$).

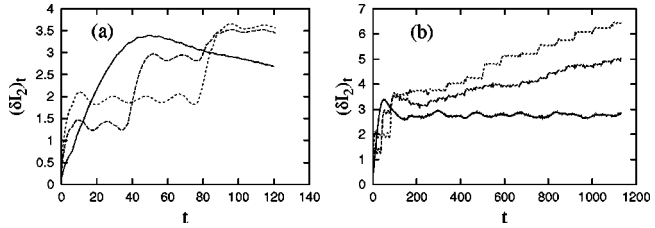


FIG. 20. $(\delta I_2)_t$ as a function of normalized time, in the case of coherent waves, for $I_1^0=1.25\times10^3$, $a_0=400$, $\overline{\nu}=30.0$, and $\alpha=2.0$, for $n_\omega=1$ (full line), 5 (broken line), and 9 (dotted line). (a) Short-term evolution; (b) long-term evolution. The initial conditions for the particles are attributed as in Fig. 18.

evolution up to $t\simeq1200$. Figure 20 also shows the progressive appearing of diffusion in the system, but the curves that display the growth of $(\delta I_2)_t$ with time exhibit smaller average inclination than in the case corresponding to one wave and $\alpha=2.0$, appearing in Fig. 19. The alternance of regions is also noticeable, regions where the curve describing $(\delta I_2)_t$ grows with time and regions where it is nearly constant and parallel to the horizontal axis. This sequence of steps is not noticeable in the one-wave case in Fig. 19.

In Fig. 21, we show $(\delta I_2)_t$ as a function of normalized time for $I_1^0=1.25\times10^3$, $a_0=400$, $\overline{\nu}=30.0$, and $\alpha=2.0$, for $n_\omega=1$, 5, and 9, for the case of waves with random phases. As in Fig. 20, panel (a) of Fig. 21 shows the evolution up to $t\simeq120$, while panel (b) shows the evolution up to $t\simeq1200$. According to Fig. 21, the initial evolution of $(\delta I_2)_t$ displays smaller inclination toward the $t$ axis than in the corresponding cases for coherent waves appearing in Fig. 20. But the long-term evolution appearing in Fig. 21(b) shows continued diffusion, without the conspicuous ''steps'' appearing in Fig. 20, in the case of coherent waves, resulting that the quantity $(\delta I_j)_t$ attains larger values in the case of Fig. 21(b) than in the case appearing in Fig. 20(b). Another interesting feature appearing in Fig. 21(b) is that the cases of $n_{wave}=5$ and $n_{wave}=9$ with random phases exhibit similar long-term behavior of $(\delta I_2)_t$, different from the behavior appearing in Fig. 20 for the case of coherent waves.

The results appearing in Figs. 19–21 are qualitatively very similar to those displayed in Figs. 10–12, indicating that the results obtained in Sec. III were not peculiar to the particular set of initial conditions for the particle coordinates utilized in that section.

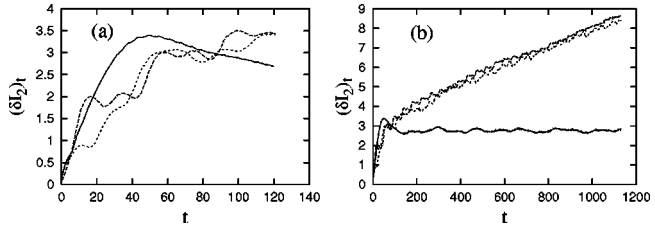


FIG. 21. $(\delta I_2)_t$ as a function of normalized time for the case of waves with random phases, for $I_1^0=1.25\times10^3$, $a_0=400$, $\overline{\nu}=30.0$, and $\alpha=2.0$, for $n_\omega=1$ (full line), 5 (broken line), and 9 (dotted line). (a) Short-term evolution; (b) long-term evolution. The initial conditions for the particles are attributed as in Fig. 18.

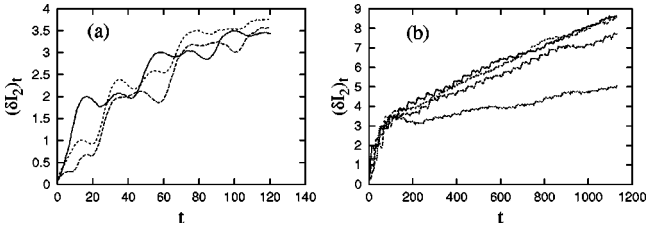


FIG. 22. $(\delta I_2)_t$ as a function of normalized time in the case of waves with random phases for $n_\omega=5$ and $\alpha=2.0$ with three different sets of random phases, obtained with different seeds for the numerical evaluation of the phases, assuming $I_1^0=1.25\times10^3$, $a_0=400$, and $\overline{\nu}=30.0$. (a) Short-term evolution; (b) long-term evolution. In panel (b), below the other three curves, the corresponding curve for the case of coherent waves is also seen. The initial conditions for the particles are attributed as in Fig. 18.

Finally, Fig. 22(a) displays the short-term evolution of the quantity $(\delta I_2)_t$, for three different sets of random phases, for $n_\omega=5$, $I_1^0=1.25\times10^3$, $a_0=400$, and $\overline{\nu}=30.0$. As in Fig. 17, we observe that, although there are differences between the three curves, the behavior is qualitatively the same in the three cases. Figure 22(b) displays the long-term evolution for the same set of parameters. The inclination of the $(\delta I_2)_t$ curve is similar in the three cases, indicating that they may be representative of the average behavior to be obtained if an ensemble average is made considering a large number of sets of initial phases. Figure 22(b) also shows the curve obtained for the case of five waves with the same phase ($\phi=0$), which displays smaller inclination toward the horizontal axis, and therefore indicates less pronounced long-term diffusive behavior.

## IV. FINAL REMARKS

We have generalized the discussion on stochastic diffusion of energetic ions by lower hybrid waves by considering a case where a set of waves with similar frequencies is present in the system. The task has been accomplished by generalizing the approach utilized in Refs. [1,2], restricting the analysis to the case of sufficiently narrow spectra, such that the phase velocity of the waves present in the system can be considered to be constant. The formulation utilized takes into account that each wave may have a random phase, with the case of coherent waves as a particular case.

The theoretical analysis of the system has shown that the initial stages of the time evolution in the case of coherent waves are ruled by a Hamiltonian similar to that appearing in Refs. [1,2], but with a threshold for stochastic behavior at the initial stages of the evolution that is smaller than the corresponding threshold obtained for the case of a single wave. In the limiting case of a continuous spectrum, with an infinite number of coherent waves, our analysis has shown that the threshold goes to zero and that the stochastic behavior at the initial stages should occur for any value of wave intensity.

When comparing the case with a single wave and the case with a finite number of coherent waves, for similar initial diffusion rate, we have shown that in the multiple-wave case the diffusion occurs in periodic bursts, which reduce the

overall efficiency of the diffusive process.

When considering the more general situation in which the waves have random phases relative to each other, the long-term diffusion obtained has been shown to be more significant than in the case of coherent waves for the same number of waves. While in the case of coherent waves the diffusive behavior occurs in periodic bursts, the diffusive behavior obtained in the case of random phases occurs continuously along the time evolution. This result is of particular interest, since the case of waves with random phases is more representative from the point of view of investigating, with a finite set of waves, the effect of a finite-width wave packet, as found in actual experiments of wave-particle interaction in tokamaks. Closer representation would be obtained by the application of an ensemble average over the initial set of random phases, a procedure that would be very costly from the point of view of numerical resources, and do not appear to be necessary in order to obtain the general features of the diffusive behavior that can be the outcome of the wave-particle interaction.

Finally we remark that the reduction of the stochasticity threshold with the increase in the number of waves, which is predicted by the present analysis, has also been obtained for different situations. For instance, for a case with two waves propagating obliquely to the ambient magnetic field [8], or for a case in which a modulation occurs in the wave frequency [12].

## ACKNOWLEDGMENTS

The authors acknowledge support from the Brazilian agencies, Conselho Nacional de Desenvolvimento Científico e Tecnológico (CNPq) and Fundação de Amparo à Pesquisa do Estado do Rio Grande do Sul (FAPERGS). Useful comments by I. L. Caldas, S. R. Lopes, R. Pakter, F. B. Rizzato, R. L. Viana, and R. R. B. Correa are gladly acknowledged.

[1] C.F.F. Karney, Phys. Fluids **21**, 1584 (1978).
[2] C.F.F. Karney, Phys. Fluids **22**, 2188 (1979).
[3] M.C.R. de Andrade, M. Brusati, and the JET team, Plasma Phys. Controlled Fusion **36**, 1171 (1994).
[4] D. Testa *et al.*, Plasma Phys. Controlled Fusion **41**, 507 (1999).
[5] L.F. Ziebell and L.M. Tozawa, Braz. J. Phys. **28**, 222 (1998).
[6] L.M. Tozawa and L.F. Ziebell, Braz. J. Phys. **28**, 211 (1998).
[7] L.F. Ziebell, Plasma Phys. Controlled Fusion **42**, 359 (2000).
[8] S. Benkadda, A. Sen, and D.R. Shklyar, Chaos **6**, 451 (1996).
[9] A.A. Vasil'ev and G.M. Zaslavskii, Zh. Eksp. Teor. Fiz. **99**, 1479 (1991) [Sov. Phys. JETP **72**, 826 (1991)].
[10] P.-K. Chia, L. Schmitz, and R.W. Conn, Phys. Plasmas **3**, 1545 (1996).
[11] D. Farina, R. Pozzoli, and M. Romé, Phys. Plasmas **1**, 1871 (1994).
[12] S. Riyopoulos, Phys. Fluids **28**, 1097 (1985).